A Multibranch U-Shaped Tunable Encoding Chipless RFID Strain Sensor for IoT Sensing System

Lan Chen, Luyi Liu, Lei Kang, Zhichong Wan, Guochun Wan, and Liyu Xie

***Abstract*—Structural health monitoring (SHM) is essential for modern large buildings and infrastructure. Radio frequency identification (RFID) widen a new paradigm for SHM in the Internet of Things (IoT) era. This article introduces a low-cost intelligent RFID monitoring system for future IoT applications. Through adding a multiparameter sensing strategy to the passive RFID tags that can be deployed on a large scale to form a sensor network, which expands the coverage of IoT in key positions health monitoring of buildings. In this work, a novel chipless RFID strain sensing tag is designed to characterize the magnitude and direction of metal surface strain, and a low-cost detection method suitable for large mechanical structures is proposed. The traditional strain antennas focus on identifying the strain characteristics without the function of encoding, and there are limitations, such as the rigid measurement methods and the expensive measurement instruments. The tag designed in this article integrates both strain sensing and encoding functions, and has the advantages of small size, high data capacity, and information reading is not easily affected by environmental noise. This article proposes an economical and flexible tag spectrum extraction method, which realizes the intelligent collection and transmission of tag data by connecting lightweight vector network analyzer (VNA) with microcontroller. Combined with the IoT, this method can be well applied to the security assessment and damage detection of large infrastructure structures, which provides a new approach to modern building health monitoring applications from integrated tag design to intelligent detection and risk assessment schemes.**

***Index Terms*—Chipless radio frequency identification (RFID) tag, Internet of Things (IoT), multiparameter on-chip integration, strain sensing, structural health monitoring (SHM), tunable encoding.**

Manuscript received 6 October 2022; accepted 10 November 2022. Date of publication 15 November 2022; date of current version 7 March 2023. This work was supported in part by the General Program of National Natural Science Foundation of China, "Research on the Principles of Passive Sensing and Structural Deformation Monitoring Methods Based on Antennas Without Stress Patch" under Project 52078375, and in part by the Top Discipline Plan of Shanghai Universities-Class I. *(Corresponding author: Guochun Wan.)*

Lan Chen, Luyi Liu, Lei Kang, and Zhichong Wan are with the Department of Electrical and Electronic Engineering, Shanghai Institute of Technology, Shanghai 201418, China (e-mail: chenlan@sit.edu.cn; 964812686@qq.com; 18232105316@163.com; asheswzc@gmail.com).

Guochun Wan is with the Department of Electronic Science and Technology, Tongji University, Shanghai 200092, China (e-mail: wanguochun@tongji.edu.cn).

Liyu Xie is with the Department of Disaster Mitigation for Structures, Tongji University, Shanghai 200092, China (e-mail: liyuxie@tongji.edu.cn).

Digital Object Identifier 10.1109/JIOT.2022.3221938

I. Introduction

STRUCTURAL health monitoring (SHM) is a technology that studies the current level of damage and strategy implementation of structures by extracting data from sensor arrays [1]. With the continuous development of modern large-scale infrastructure, industrial, and transportation systems have become more and more complex, and a large number of complex metal structures, such as steel-frame buildings, pipelines, wind turbines, power plants, aircraft, etc. will suffer wear and tear once they are delivered [2]. Although these structures are designed to carry heavy loads and operate for a long time, due to the uncertainty of the working environment, metal materials are vulnerable to cyclic loads and chemical erosion, resulting in deterioration phenomena, such as strain, corrosion, and cracks. Different degrees of damage of mechanical structures will affect the change of mechanical properties of load-bearing materials, and the main characteristic of structural damage in the early stage is the strain degree of the structure [3]. Therefore, it is particularly important to respond to catastrophic risks of large infrastructures as early as possible through SHM.

The intelligent SHM system plays an indispensable role in the development and construction of smart cities [4]. In the past, in SHM systems, the structure of the facility was regularly inspected by nondestructive testing (NDT), such as visual, ultrasonic, and electromagnetic (EM) testing assessment techniques [3], [5]. However, most of the SHM systems used in industry are active wired systems. Considering the volume and complexity of large structures, the deployment, maintenance, and debugging of wired SHM systems are very troublesome, meanwhile, the supporting monitoring instruments are high cost, long flaw detection time, and short data transmission distance, which restrict the further development of the technology [6]. Therefore, a passive wireless intelligent monitoring network for SHM system that can realize long-distance and low-power data transmission is proposed, which can greatly alleviate the current predicament. It is worth noting that with the rapid development of the Internet of Things (IoT) era in recent years, chipless radio Frequency (RF) Identifier technology has opened a new paradigm, especially the combination of information sensing and the IoT. It has greatly stimulated the new potential in the SHM field [7].

The IoT is regarded as the future of the Internet, with embedded and complex sensing and driving capabilities [8].

As a key IoT implementation technology, RF identification (RFID) plays an important role in the future development of SHM systems. RFID was originally proposed as a substitute for optical barcodes, which modulates signals through RF chips to form unique identifiers to identify objects and information sensing [9]. In the field of SHM, the cost of RFID system mainly depends on the cost of lots of deployed RFID tags, so the existence of chips restricts the optimization space of its cost [10]. Chipless RFID is a passive wireless, contactless automatic identification and tracking NDT solution with lower cost and higher benefits. The technique uses RF waves to identify remote chipless tags and extract encoded information stored in the tag notch circuit structure from the backscattered waves. Compared with chip RFID tags, chipless RFID tags do not contain RF silicon chips and additional integrated circuits in their structure, so no additional power supply is required, and they can be effectively deployed in economically underdeveloped places [11].

The chipless RFID tag sensor has been widely studied because it does not require an additional power supply and can realize the information sensing of the characteristic parameters through the wireless layout in economically backward areas. The chipless RFID antenna sensor can take advantage of the characteristic that its resonant frequency shifts with its size deformation. By detecting the changes of characteristic parameters under RF excitation, the size changes and the strain received by the antenna are calculated and estimated. In the initial period, the rectangular patch antenna (RPA) with chip was used as a strain sensor, which could be used to detect stress and gap on the surface of the specimen at the same time. Yi et al. [12] designed a slotted patch antenna with chip for strain and crack sensing, and adopted RFID chip for signal modulation, and the operating power of the RFID chip is obtained from the interrogation signal of the wireless reader. After that, Cho et al. [13] made improvements and added a Schottky diode configuration network to the antenna radiation surface, which removed the limitation of the chip and reduced the mutual influence between signals. Herbko et al. designed a variety of fractal structure chipless RFID rectangular patch for performance comparison. By setting the same strain sensing operating frequency, the influence of the initial resonant frequency on the sensitivity of the patch tag was eliminated. The results showed that the higher the number of fractal iterations, the lower the sensor sensitivity. Therefore, the regular rectangular microstrip patch antenna has the best strain sensing performance [14]. When the metal structure is exposed to the external environment for a long time, in addition to the damage of the early strain, the erosion of the climate environment will also cause the skin corrosion of the metal structure, and even cause cracks of different degrees [15]. In the context of SHM, if chipless RFID sensors can be deployed to safety-critical areas of large structures on a large scale, protection effects like smart skin can be formed. Dey et al. [16] designed a waveguide-based split-box resonator that can identify cracks in the structural areas of buildings as well as moisture on the dielectric substrate. Sameir Deif and other scholars in Canada designed a multiresonance chipless RFID array system for pipe coating defect detection and corrosion prediction. By predicting corrosion before it occurs, proactive responses can be taken to mitigate the possibility of environmental disasters [17].

Despite the advantages of the chipless RFID technology for SHM, it is still under intensive research. The size and encoding capacity of chipless RFID tags is currently one of the main challenges to reduce the cost of tags [18]. With the development of the sensors and micromachining technology, sensors are developing towards multifunctional applications, and sensors with multiparameter integration have gradually become a research hotspot [19]. Chipless RFID tags have the advantage of being printable and embeddable, which makes it easier to integrate sensors into materials. Another advantage is that information can be encoded using resonance in a broadband frequency range, and multiresonance can allow chipless RFID to detect multiple physical variables simultaneously, which incorporates more sensing functions into the frequency characteristics of the sensor. When there are lots of sensors in the environment, it is important to distinguish the identity information of sensors. The identification of a single sensor can be effectively realized by adding the ID coding function. Many scholars have made exploratory attempts to perform multifunctional integration of sensing and tag identification. Abdulkawi et al. proposed a compact, high encoding capacity resonator equipped with (k-1) arms within a U-shaped coupled microstrip framework, where one isolated arm was designed to individually connect the U-shaped framework to tune its resonant frequency, so each resonator can be tuned to a total of k different frequencies. And then, Abdulkawi and Sheta [20], [21] proposed a new microstrip coupled line resonator that can simultaneously supports four-state ID data and additional temperature sensing information. Marindra and Tian [22] first proposed a 4-bit code-integrated strain sensor that realizes the band-partitioned characterization of structural strain and identity information, which provided an interesting design idea for increasing the function of chipless strain sensors.

The application of flexible strain sensors in human wearable electronic systems is a hot research topic. However, most of the reports focus on the monitoring of human structural health [23]. If the design of flexible strain sensors can be widely used in the field of SHM of infrastructure facilities, using the soft and flexible characteristics of the sensor to allow them to closely fit with curved structures, which will greatly improve the engineering applicability of chipless RFID antenna sensors. In actual engineering deployment, if the size of the chipless tag is too large to fit on the complex structure surface, it is a wiser choice to choose a flexible substrate [24]. Pan et al. designed and fabricated a flexible, stretchable, and compact split complementary resonant (SRR) ultrahigh frequency (UHF) RFID antenna based on liquid conductive materials, which is converted into the change of structural stress parameters through the resonant frequency shift of the antenna [25]. Chao et al. designed a micro-strain sensor based on the interdigital capacitance structure, which can be effectively attached to the surface of the structure and can stretch or bend as the structure deforms, so that it can detect small mechanical changes in the structure compared to the original state, to facilitate real-time monitoring, a wireless

system was also designed and implemented to integrate sensors for remote SHM applications [26]. Although the literature on chipless sensing tags have been widely reported, there is still no convenient and efficient intelligent detection scheme. Furthermore, the exploration of versatile chipless RFID sensing applications is currently focusing on environmental climate change monitoring sensors, such as temperature, humidity, and gas sensors [27]. So far, there is not enough research on multifunctional chipless RFID sensors that simultaneously examine structural strain and characterize encoding in the field of SHM, and no effective intelligent detection and wireless transmission strategy has been developed for sensor data extraction. Therefore, designing and developing multifunctional chipless RFID sensors and their intelligent detection methods for structural strain and information encoding is an engineering problem worth exploring.

This article reports a novel passive RFID integrated sensor for wireless interrogation and monitoring of strain in metallic samples. The fabricated RFID sensors were tested for strain sensing on commercial aluminum plate specimen. Section II introduces the integration process of the RFID tag, the 3-D electromagnetic model, and its parameter design optimization. Section III tests the tag characterization of multiple groups of aluminum specimen samples, compares wired measurement and retransmission wireless measurement, and verifies the feasibility of lightweight VNA testing engineering strain. Section IV discusses the further integrated application prospects of passive RFID tags and the possible scheme for encoding electronic tuning. Section V presents a low-cost chipless RFID tag intelligent detection scheme applied to the IoT. Finally, the conclusion and the future study directions are given in Section VI.

II. Chipless RFID System Operating Principle

A. Chipless RFID System Communication Theory

A typical chipless RFID system communication as shown in Fig. 1 includes: chipless RFID sensor, reader part, and backend processing part. Its working principle mainly uses RF signal as the medium to realize the identification and detection of the target object. The reader transmits or conducts RF signals to form a certain range of electromagnetic fields in space [19]. When the chipless RFID tag enters an area with a strong enough excitation signal, the tag receives the excitation signal from the reader and generates energy. The excitation signal is influenced by the special structure of the tag to form a signal with specific characteristics and then return to the reader. Finally, it is sent to the computer terminal through the reader for serial processing and analysis of the signal.

B. Chipless RFID Coding Theory

In recent years, stable and high-capacity chipless RFID encoding methods have been researched and proposed. There are two main types of data encoding for chipless RFID tags: 1) time domain reflectometry (TDR)-based tags and 2) frequency domain (FD)-based tags. Chipless RFID tags

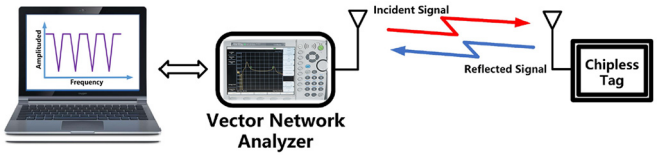

Fig. 1. Working principle of the chipless RFID system.

based on TDR send signals in the form of pulses from the reader and receive the pulse echo sent by the tag to conduct inquiry. A series of simple pulses can be created to encode the data. The disadvantage is that the price is high, the design is limited by its material properties, the further expansion of the encoding capacity is restricted, and the reader has higher requirements on the orientation and moving speed of the tag, which is not conducive to the further development of mobile detection methods. Therefore, most of the research on the size of miniaturized RFID tags and the capacity of extended data are based on FD systems [28].

In FD-based chipless tags, data can be encoded using resonators, each resonator absorbs part of the transmitted power at a specific frequency, forming a corresponding band-stop filter on the frequency band, so each resonator can correspond to a resonance in the spectrum frequency. The logic of the code bit corresponding to the resonance frequency is defined as "1" state, and when the corresponding work frequency band has no band-stop filtering, the code bit logic turns to "0" state.

Chipless tags based on the FD are generally classified into two types: 1) backscatter and 2) retransmission. Backscatter-based chipless tags rely on the self-resonance of multiple resonators to generate spectral properties for encoding, with the advantages of being small, easy to read, and no additional Tx/Rx antennas are required. However, the performance of backscattering tags is strongly dependent on the specific shape of the multiresonant elements, and when multiencoding elements are added to increase the information capacity, the significant coupling is introduced, while for chipless RFID strain sensors, the tag is closely related to the coupling of strain elements is a fatal flaw, which seriously affects the reliability of strain information. The retransmission chipless tag consists of two cross-polarized antennas and a multiresonator that stores data, and it can significantly reduce interference between transmitted and received signals using two orthogonally polarized transceiver antennas. According to the polarization characteristics of the background scattering signal, the electromagnetic characteristics can be used for calibration [29]. Most importantly, by adjusting the distance between different resonant units, the coupling interference between the units is basically eliminated. The working principle of a chipless RFID strain sensor based on spectrum signature is shown in Fig. 2. The sensor is composed of a transmitting antenna, a receiving antenna and a chipless RFID strain sensor. Among them, a chipless RFID strain sensor constitutes a two-port network, which uses a notch circuit to realize spectrum signature. It should be noted that the working range of broadband antenna is larger than the working bandwidth of a chipless two-port network.

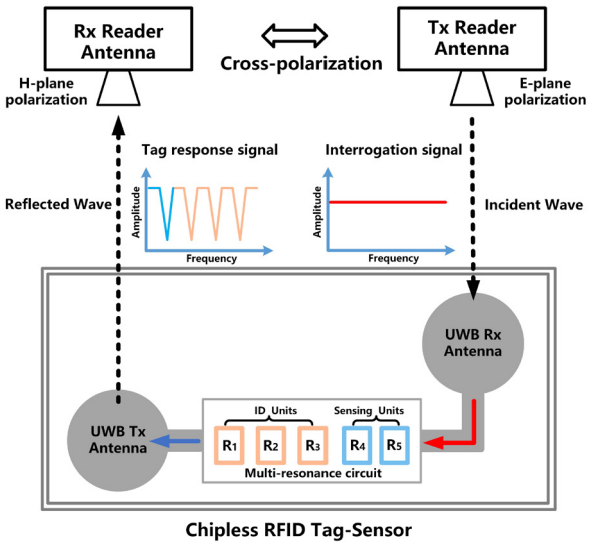

Fig. 2. Working principle of the integrated strain sensor.

III. Tag Antenna Design and Sensing Principles

In this part of this article, a retransmission-based multistate encoding strain antenna sensor is proposed. The sensor is used for metal structure defect detection, and the bottom of the tag is designed with a metal ground plate so that the electromagnetic characteristics do not change significantly when approaching metal [30]. Due to the use of a main 50-Ω microstrip line, this tag can flexibly adjust the distance between different resonant units, which reduces the coupling interference between different resonant units. In addition, the orthogonally polarized transceiver antenna provides a high degree of isolation between the received and transmitted signals of the tag, which improves the accuracy of reading data.

A. Tag Antenna On-Chip Integration Geometry

As shown in Fig. 3, this article proposes an on-chip integrated multifunctional tag antenna. This tag uses a U-shaped band-stop resonator unit with multibranch, which has the advantages of high Q-value, high spectral efficiency, high encoding capacity, etc. Meanwhile, the tag additionally integrates a strain sensitive RPA and the element is used to monitor the strain of the structure. This integrated tag has strain sensing and 4-bit compact encoding functions, and its main structure includes: an upper radiating surface, a dielectric substrate, and a ground plane for metal installation. Among them, the upper radiating surface is composed of a main microstrip line connecting two-ports network, a rectangular patch resonant unit, and four microstrip coupling multibranch U-shaped resonators, and the dielectric substrate is Roger 5880 ($\varepsilon_r = 2.2$, $h = 0.78$ mm, and $\tan\delta = 0.0009$). In the integration of multiple resonators on the tag, the priority should be to consider that each element on the tag should be combined into a complete structure. At the same time, in order to reduce the cost of the tag, the size of the tag antenna should not be too big when increasing the resonator unit. Therefore, the coupling effect between the resonant elements should be minimized by reasonable optimization of the layout. When the tag is subjected to structural strain, ideally, the strain measurement part should be able to undergo linear frequency variation as theoretical reasoning, while the resonant frequency of the encoding unit part remains stable.

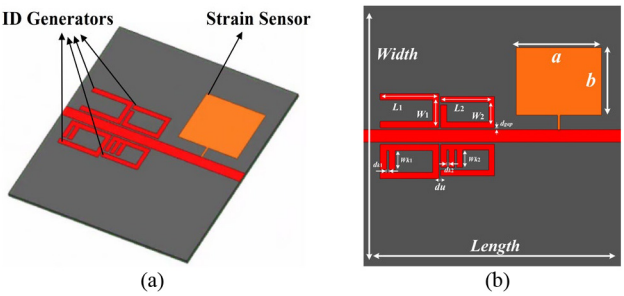

Fig. 3. Geometry of the proposed tag antenna. (a) 3-D model. (b) Front view.

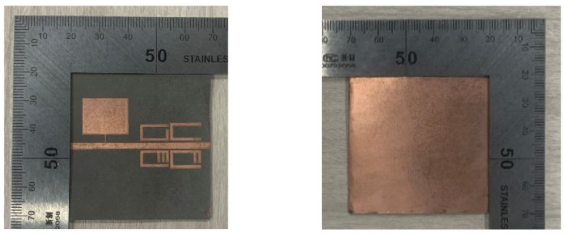

Fig. 4. Fabricated integrated sensor tag. (a) Radiating surface. (b) Metal mounting surface.

TABLE I
Main Parameters of the Integrated Sensor

Parameter	$L1$	$L2$	$W1$	$W2$
Value (mm)	11.28	10.34	6.60	6.05
Parameter	$Wk1$	$Wk2$	$dk1$	$dk2$
Value (mm)	3.60	3.30	0.48	0.44
Parameter	$dgap$	du	$Length$	$Width$
Value (mm)	0.40	0.40	50	50

The proposed integrated sensor is designed and optimized in the high-speed RF simulation software ANSYS, and the complete layout is shown in Fig. 3(a) and (b) is the front view of the tag antenna. Some important parameter symbols are marked in Fig. 3(b), and the recommended design dimensions of the main parameter dimensions are given in Table I. The overall size of the integrated sensor is 50 mm × 50 mm × 0.78 mm.

Fig. 4 shows the physical picture of the tag, which obtained by thermal transfer printing and printed circuit board (PCB) etching under laboratory conditions. This tag uses a low dielectric constant substrate Rogers5880. This high-frequency laminate has excellent pressure resistance and can withstand large forces, so it can ensure that the tag will not be torn at large strain values. In addition, the substrate has low water absorption and chemical resistance, which allows continuous operation in humid and harsh environments and reduces the loss of tag performance caused by climate factors. The measurement of this tag is carried out with the PNA, and the

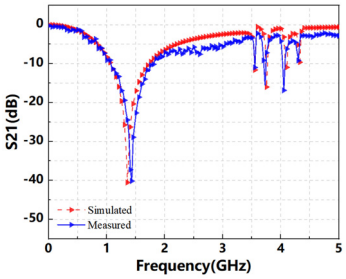

Fig. 5. Simulate and measure responses of fabricated integrated sensor tag.

measurement results together with the simulation results are shown in Fig. 5.

This tag can generate five resonant frequencies, which is designed with a 4-bit encoding area and a 1-bit strain sensing area. The S21 resonant frequency generated by the patch antenna is 1.38 GHz, and the return loss is as high as −40 dB, which is used for strain sensing function. Other resonant points with higher frequencies are used to encode the tag's identity information. There is an isolation of 1.17 GHz between the working bandwidths of the two functional areas, and each function is quantized within its own working frequency band without interfering with each other.

B. Encoding Unit Design and Selection Criteria

The application of coded tags in RFID systems has promoted the IoT developmentError! Reference source not found. By adding encoding to sensors, sensor tags tracking in many deployed sensor networks can be achieved. Fig. 6(a) is a coupled U-shaped resonator, Fig. 6(b) is a coupled spiral resonator, Fig. 6(c) is the frequency response curve of U-shaped resonator and its equivalent circuit model and Fig. 6(d) is the frequency response curve of a spiral resonator and its equivalent circuit model. Different notch curves are created by adding these resonators to the microstrip transmission line and these resonance curves indicate that the logical state of the data bit carried by the chipless RFID tag is "0" or "1."

The microstrip coupled U-shaped resonator is a resonant structure with a high Q-value. Compared with the existing spiral resonant structure, the U-shaped resonator has more compact bandwidth, so more resonance unit can be settled in the same frequency band. Fig. 6(a) and (b) marked the main parameter dimensions of the U-shaped resonator and spiral resonator coupled with microstrip lines. This work uses Rogers 5880 as the dielectric substrate and is designed in the RF simulation software ANSYS. Fig. 6(c) and (d) shows the equivalent models of the lumped circuit elements corresponding to the U-shaped resonator and the spiral resonator, respectively. The simulation results show that the designed coupled U-shaped resonator unit forms a good band-stop resonance curve at 2.72 GHz, and the transmission coefficient S21 is about −16.6 dB. The spiral resonator produces two resonance frequencies with band-stop characteristics of −9.5 dB at 1.65 GHz and −12.3 dB at 3.56 GHz. When the design dimensions of the two resonators are close, the spiral resonator unit has a longer microstrip line, so the resonance frequency is lower than that of the U-shaped resonator. However, the

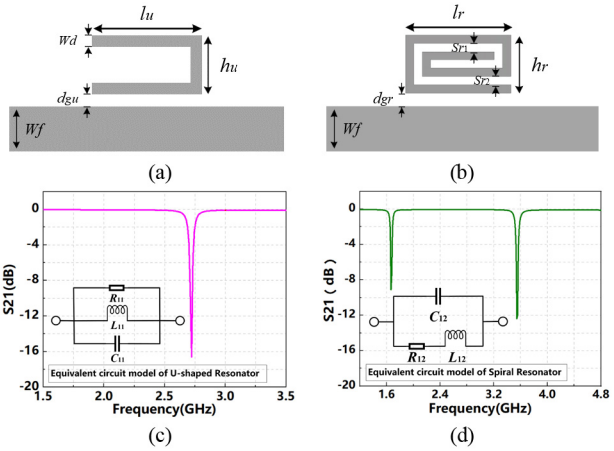

Fig. 6. (a) Geometry of U-shaped resonator (lu = 18.75 mm, hu = 6.875 mm, dgu = 0.35 mm, Wd = 1.25 mm, Wf = 2.4 mm). (b) Geometry of Spiral resonator (lr = 18.75 mm, hr = 6.875 mm, dgr = 0.35 mm, $Sr1$ = 1.25 mm, $Sr2$ = 1.25 mm, Wf = 2.4 mm). (c) Frequency response curve and equivalent circuit model of U-shaped resonator. (d) Frequency response curve equivalent circuit model of spiral resonator.

winding microstrip line of the spiral resonator makes the resonant structure complicated, so the microstrips are easy to mutual coupling interference, resulting in unnecessary resonant frequencies. The resonant bandwidth of the U-shaped resonator is about 14 MHz, which is smaller than the 19-MHz bandwidth of the spiral resonator, so the notch curve is more compact, and the return loss of the U-shaped resonator is higher, which is easier to be captured by the detection equipment.

The band-stop resonance characteristics of the resonator can be simulated by lumped circuit elements, where the $L11$, $C11$, and $R11$ equivalent elements generate the resonant frequency of the U-shaped resonator, and the $L21$, $C21$, and $R21$ equivalent elements generate the resonant frequency of the spiral resonator. The equivalent circuit parameters of the U-shaped resonator can be determined by (1)–(3), which provides a reference for the design process of the resonant frequency of the subsequent resonator [10]

$$C = \frac{\omega_c}{2Z_0(\omega_0^2 - \omega_c^2)} \tag{1}$$

$$L = \frac{w_c}{4\pi^2 f_0^2 C} \tag{2}$$

$$R = \frac{2Z_0}{\sqrt{\frac{1}{(S_{11}(\omega_0))^2} - \left(2Z_0\left(\omega_0 C - \frac{1}{\omega_0 L}\right)\right)^2 - 1}} \tag{3}$$

where ω_0 is the angular resonance frequency, ω_c is the 3-dB cutoff angular frequency, and Z_0 is the characteristic impedance of the microstrip line.

In recent years, the encoded tag antennas with multistate coupled lines have gradually attracted the attention of scholars. This type of tag can change the radiation characteristics of resonator by flexibly combining microstrip lines. This method is similar to "pruning and restoring branches in a tree." In a stable microstrip structure, adjusting the branch microstrips of each part achieves the purpose of adjusting the frequency shift of the resonator. The advantage is that the combination

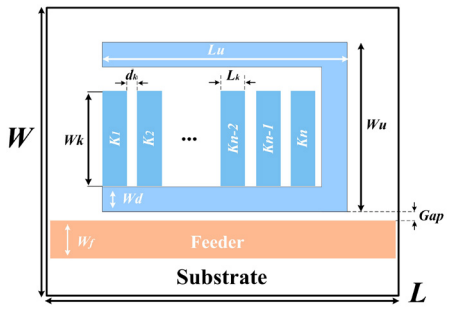

Fig. 7. Multibranch U-shaped resonator model.

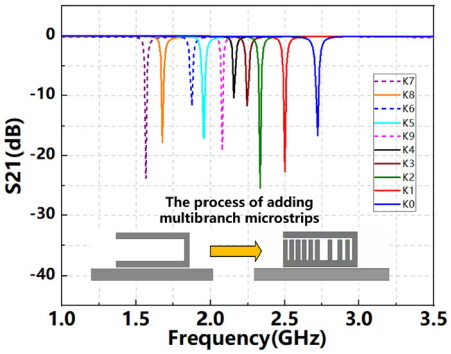

Fig. 8. Multibranch addition process and its corresponding frequency response.

is flexible and the resonance state can be adjusted without making major shape changes to the resonator, which is different from the traditional method of generating different resonance frequencies by changing the radiation length of the spiral microstrip. Since the encoding state of the chipless RFID tag based on the coupled U-shaped resonator is single, this article proposed a multibranched resonator based on coupled U-shaped microstrip frame. By connecting branch arms inside the U-shaped resonator, n frequency shifted states, and $(n+1)$ resonant frequencies for a single resonator are realized. Fig. 7 shows the improved multibranch U-shaped resonator model, which has the characteristics of small size and large encoding capacity.

When a metal branch arm $K1$ is connected to the U-shaped microstrip groove, the resonant frequency of the original resonator will be shift to a certain degree. With the continuous increase of branches, more states can be generated so that each resonator has a larger encoding capacity. The length of the two arms of the coupled U-shaped groove is Lu, the dimension of the bottom is Wu, the width of the groove is Wd, the length of the bottom of the branch in the U-shaped groove is Lk, the dimension of the arms is Wk, and the distance between adjacent branches is dk. These three parameter dimensions in (4) mainly determine the shift of the resonator frequency

$$\begin{cases} f_n = f(dk, Lk, Wk) \\ \Delta f = f_0 - f_n \end{cases}. \tag{4}$$

Designing the dimension of branch K, where $Lk = 3.95$ mm, $Wk = 1.05$ mm, and $dk = 0.55$ mm. The simulation is carried out in ANSYS software, and the distance dk between

TABLE II
POSSIBLE RESONANT FREQUENCY STATES OF A SINGLE RESONATOR

State (n)	Branch Connected to frame	Identity of Each Unit	Frequency (GHz)	Δf (GHz)
1	None	f_0	2.72	0.00
2	1	f_1	2.50	0.18
3	2	f_2	2.33	0.39
4	3	f_3	2.24	0.48
5	4	f_4	2.17	0.55
6	5	f_5	1.96	0.76
7	6	f_6	1.87	0.85
8	7	f_7	1.56	1.16
9	8	f_8	1.67	1.06
10	9	f_9	2.07	0.65

adjacent branches is kept equal. With the increase of branches, the state of $n = 1$ to $n = 7$ presents good frequency shift characteristics and the resonant frequency gradually decreases. However, when increasing to seven branches, the resonant frequency of the corresponding $n = 8$ state does not decrease continuously, and it can be observed that the branch spacing parameter dk can be adjusted to achieve the desired resonant frequency. Therefore, this work achieves more branch configurations by adjusting the dimension of the parameter dk, thereby realizing more frequency shift states of the resonator, and further expanding the code capacity that the resonator can carry. Fig. 8 shows the process of adding branches in the coupled U-shaped resonator and the resonance response curves under different n states are obtained by simulation.

When the configuration of branches in a single coupled U-shaped resonator unit reaches a larger number, the effect of the frequency shift will be reduced. The resonator has a high current distribution at the bottom of the U-shaped groove, so as the branches gradually increase and close to the bottom of the U-shaped groove, they will be affected by the coupling. Adjusting the distance between adjacent branches can optimize the effect of the coupling on the frequency shift. The frequency characteristics of a single resonant unit obtained after optimization in ANSYS are summarized in Table II. This scheme can give full play to the advantages of the high Q-value of the U-shaped resonator, achieve the maximum utilization of the spectrum in a small working frequency band, and at the same time the physical space occupied by the resonator will not increase.

In this work, the proposed 1-bit chipless RFID tag has ten frequency position encoding capabilities in the working frequency band, and the encoding mode is flexible. There are C_{10}^{8} (45) options in a single resonant unit that can be used for 3-bit binary information encoding. If there are N resonant units, the amount of encoding data that may be reach 10^N. The proposed technology allows this resonator to carry higher bit encoding capabilities in the same tag dimension. In addition, expand or shrink the dimension of the tag can also obtain a different resonant frequency.

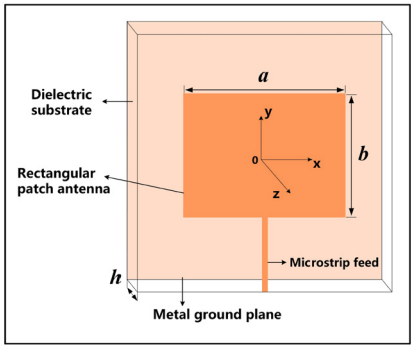

Fig. 9. Geometry of RFID patch antenna.

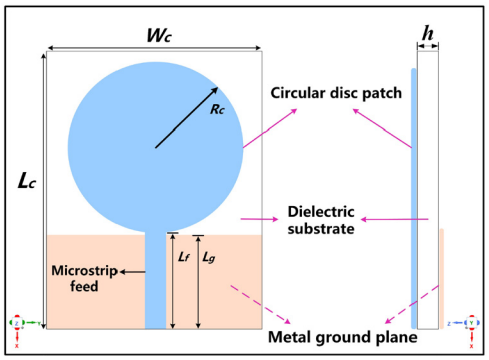

Fig. 10. Geometry of disc monopole antenna.

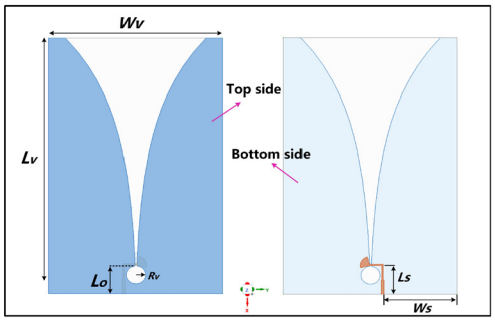

Fig. 11. Geometry of reader antenna.

C. Rectangular Patch Strain Sensing Unit Design

In the emerging field of SHM, chipless microstrip antenna strain sensors based on the RFID technology have become a research direction due to their low cost and large-scale deployment characteristics. Chipless microstrip sensors do not require additional power supplies and can be flexibly attached to large structural components under test in underdeveloped areas. When the stress is transmitted to the sensor, the structural deformation changes the geometry of the tag resonant unit, thereby affecting the corresponding resonant frequency change.

The RFID RPA has the characteristics that the resonant frequency changes with the dimension. The degree of change in the size of the patch antenna can be characterized by the degree of resonant frequency shift of the patch antenna, and then the degree of deformation of the measured object can be characterized. Fig. 9 shows the transmission line model of the rectangular patch. The main body of the rectangular microstrip patch antenna has two main parameters, length b and width a, and its dimensions can be calculated, respectively, as follows:

$$a = \frac{1}{4f_r\sqrt{\mu_0\varepsilon_0}}\sqrt{\frac{2}{\varepsilon_r+1}} = \frac{c}{2f_r}\sqrt{\frac{2}{\varepsilon_r+1}} \tag{5}$$

$$b = \frac{1}{2f_r\sqrt{\varepsilon_e}} - 2\Delta L \tag{6}$$

where fr is the initial resonant frequency of the antenna, μ_0 is the magnetic permeability in a vacuum, c is the speed of light in a vacuum, ε_0 is the dielectric constant in a vacuum, ε_r is the relative permittivity of the dielectric substrate, and ε_e is the equivalent dielectric constant of the dielectric substrate electric constant, ΔL is the compensation length.

The relationship between resonant frequency and antenna length can be deduced in (7) as follows:

$$f_r = \frac{c}{2(b+2\Delta L)\sqrt{\varepsilon_e}}. \tag{7}$$

It can be seen that the resonant frequency of the rectangular patch is mainly related to the dimension of parameter b, thereby the patch antenna has higher sensitivity in the longitudinal direction. This work designs an RFID RPA as a strain sensor applied in the SHM field. Its principle is to use the characteristic parameters of RFID antenna will change with the change of its dimension and calculate the dimension change and the strain of the antenna by detecting the evolution of the characteristic parameters under the radiofrequency excitation.

D. Ultra-Wideband Transceiver Antenna Design

The RFID communication between the chipless reader and the tag antenna can be realized by designing the corresponding ultrawideband (UWB) transceiver antenna. The design bandwidth of the UWB antenna should cover the entire encoded spectrum to obtain the many frequency signatures required for the high capacity of data bits carried by the sensor. As shown in Fig. 10, the designed UWB monopole antenna is used to connect the two-port network of the tag sensor to send and receive signals. With the advantages of omnidirectionality and easy flat printing, this UWB monopole antenna can be integrated with the proposed tag sensor flexibly.

However, the traditional disc monopole antenna has the shortcomings of low gain and short wireless retransmission distance, which limits the application of the sensor in engineering. Therefore, in order to increase the reading distance of chipless readers, it is necessary to design a high gain directional antenna for the RFID reader, Fig. 11 shows the geometry of the proposed Vivaldi antenna [31].

In general, the two UWB antennas often interfere with each other during operation bandwidth. In order to overcome the problem of communication crosstalk, the linearly polarized antenna used in this article can effectively alleviate this problem by placing it orthogonally. Orthogonal cross-polarization can act as an isolation mechanism between the interrogation signal sent by the chipless reader and the tag response signal received by the chipless reader, enabling

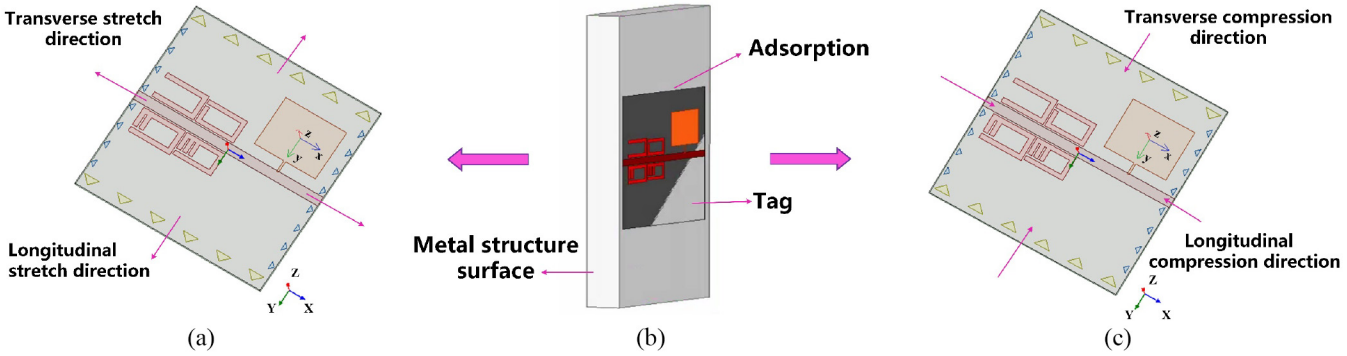

Fig. 12. Integrated sensor strain transfer process. (a) Transverse process interpretation. (b) Tag installed to metal surface. (c) Compression process interpretation.

TABLE III
MAIN PARAMETERS OF THE UWB TRANSCEIVER ANTENNA

Parameter	*Lc*	*Wc*	*Lv*	*Wv*
Value (mm)	80	70	114.5	72
Parameter	*Rc*	*Rv*	*Lf*	*Lg*
Value (mm)	22	4	33	32.5
Parameter	L_0	*Ls*	*Ws*	
Value (mm)	12.48	13.5	30.47	

efficient transmission of the tag's characteristic spectral signatures. In addition, the main parameter dimensions of UWB antenna are given in Table III.

IV. SENSOR STRAIN SCENARIO SIMULATION AND TENSILE EXPERIMENT

A. Strain Characteristic Analysis of Integrated Sensors

To evaluate the strain characteristics of the integrated sensor to be designed, some simulation analyses are required. According to the previous derivation, (7) shows that there is a certain relationship between the size of the rectangular microstrip patch and the resonant frequency. When the sensor is strained, the thickness of the substrate plate and the width of the radiation patch also change when the longitudinal strain increases due to the Poisson effect [32]. Taking the Poisson effect into account, it is possible to further calculate the relationship between the resonant frequency shift of the antenna and the strain.

The effect of force on the strain of the integrated sensor is simulated in ANSYS. The transverse strain stretching of the sensor is shown in Fig. 12(a), the sensor deployed on the surface of the metal structure is shown in Fig. 12(b), and the transverse strain compression of the sensor is shown in Fig. 12(c). The sensor is tightly attached to the surface of the metal structure by using high-performance adhesive. When the metal is deformed by strain, this effect is synchronized to the tag's substrate, and at this time, the sensor starts to work. When the substrate is transversely strained, the force is along the x-axis horizontal direction, when the substrate is longitudinally strained, the force is along the y-axis horizontal direction, and the variation direction of the substrate thickness is consistent with the z-axis.

Assuming that the rectangular microstrip patch is deformed in the transverse direction, the patch will be strained along the x-axis direction, and the length along the x-axis direction is changed from the initial length a_0 to a_s, and the degree of deformation is set as φ_a, $\varphi_a = (a_s - a_0)/a_0$. However, considering that the actual change is not in a single direction, according to the Poisson effect, when stretching along the x-axis direction, the y-axis and z-axis directions will also be compressed to a certain extent. The thickness of the substrate is much smaller than the length and width of the rectangular patch, so its influence is ignored here. The strained relationship in the y-axis direction of the rectangular patch is given in (8) as follows [33]:

$$b_r = b_0(1 - \nu\varphi_b) \tag{8}$$

where b_s is the length of the rectangular microstrip patch after straining, b_0 is the initial length before straining, and ν is Poisson's ratio constant, which is set to 0.3. Substitute the strain and Poisson formulas into the calculated (8) for the resonant frequency of the rectangular patch that has been derived, and simplification can be obtained in (9) as follows:

$$f_r(\varphi_a) = f_0(1 + \nu\varphi_a) \tag{9}$$

where f_s is the rectangular patch's frequency shift after the strain of φ_a, and f_0 is the initial frequency. It is also possible to calculate the frequency shift after the rectangular microstrip patch is deformed in the longitudinal direction in (10) as follows:

$$f_s(\varphi_b) = f_0(1 - \varphi_b). \tag{10}$$

Therefore, theoretically, when the RPA is subjected to transverse or longitudinal strain, its resonant frequency will shift linearly. The resonant frequency increases with increasing force during transverse stretching. The resonant frequency decreases with increasing force during longitudinal extension. On the contrary, the resonant frequency decreases with the increase of force in transverse compression and the resonant frequency increases with the increase of force during longitudinal compression. Therefore, the linear by analyzing change of resonant frequency, the strain magnitude and direction of the antenna can be inferred. Then, the strain of the measured structure attached to the antenna can be calculated, which provides theoretical guidance for the following simulation verification.

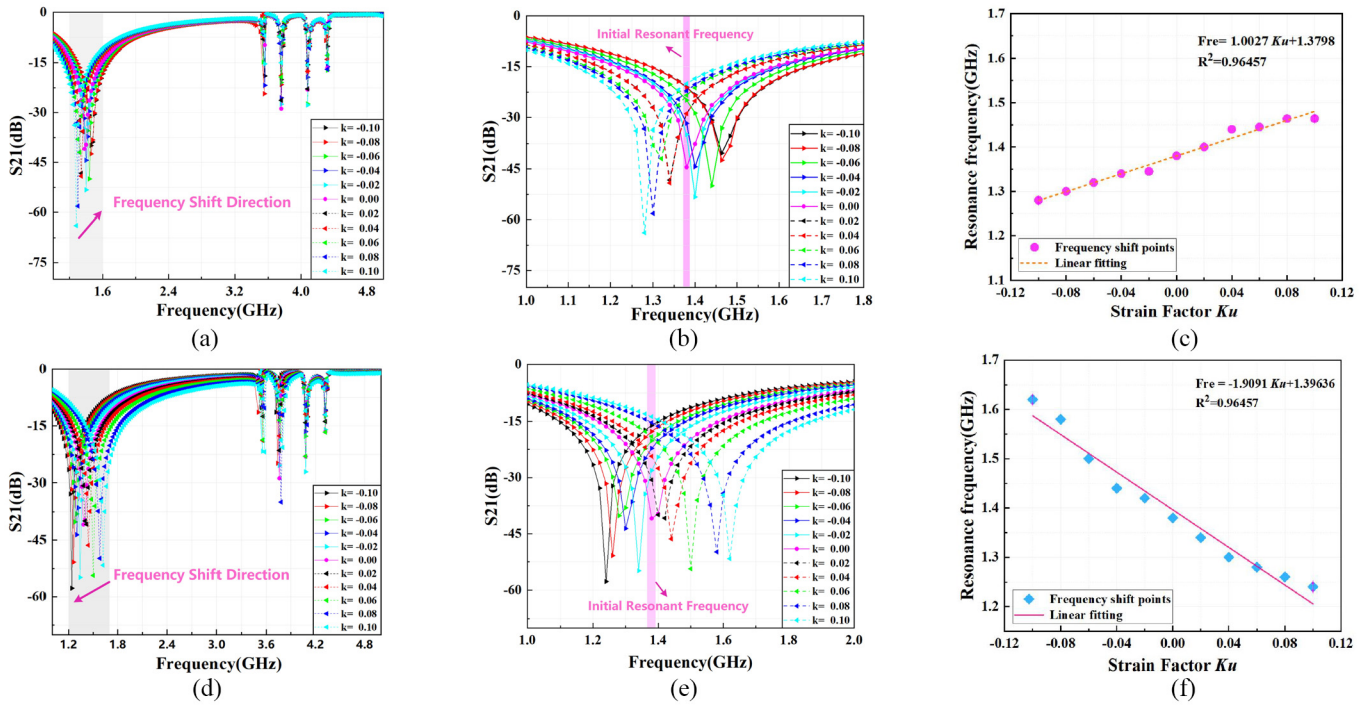

Fig. 13. (a) S21 curve of the RFID sensor after transverse strain. (b) S21 curve of transverse strain frequency shift in enlarging part. (c) Linear fitting line of transverse strain frequency shift. (d) S21 curve of the RFID sensor after longitudinal strain. (e) S21 curve of longitudinal strain frequency shift in enlarging part. (f) Linear fitting line of longitudinal strain frequency shift.

To verify the above inference, variable K_u as a strain factor is set in ANSYS software to represent strain degree, and Poisson's ratio constant is set to 0.3. Setting the variation range of K_u as $(-0.10, 0.10)$ in the overall integrated sensor simulation model, and set 0.02 as step size to simulate the strain situation in both longitudinal and transverse directions. In addition, K_u is positive to simulate the strain stretching degree, K_u is negative to simulate the strain compression situation, and $K_u = 0$ means that there is no strain action. The initial resonant frequency of the rectangular microstrip patch is about 1.38 GHZ and considering the Poisson effect, the obtained strain simulation results are shown in Fig. 13.

When the RFID integrated sensor is subjected to stress, the antenna size will change, so the sensor units will change to different degrees. It can be observed in Fig. 13(a) and (d), the resonant frequency with the most minor is the response corresponding to the strain sensing unit and the other higher frequency regions are the resonant frequencies of the encoding units. After the simulating strain in ANSYS, the resonant frequency of the rectangular microstrip patch has a significant shift, which is consistent with the previous theoretical conclusion. By contrast, the resonant frequency shift of the encoding units is very small, which has strong stability and anti-interference. Fig. 13(b) and (e) shows the frequency shift of the integrated sensor strain sensing unit after enlarging part, and the pink area marked in figure is the 1.38-GHz initial frequency. The resonant frequency of the rectangular patch varies linearly and uniformly with the increase of strain degree. To verify and calculate the resonant frequency shift characteristics of the strain sensing unit, the frequency shift of the strain unit was fitted by linear normalization, and the fitting result was shown in Fig. 13(c) and (f). Among them, Fig. 13(c) is the fitting line of transverse strain resonant frequency change of the rectangular patch part of the integrated sensor and Fig. 13(f) is the fitting line of longitudinal strain resonant frequency change. Therefore, the fitting lines show that the variation trend of the resonant frequency of the rectangular patch part and the strain in different directions is approximately linear. In Fig. 13(c), the fitting line has an intercept of 1.39636 GHz, which has a certain deviation from the initial frequency of 1.38 GHz, and then the strain factor was converted into micro-strain units with a sensitivity of 1.00273 kHz/$\mu\varepsilon$. The fitting line in Fig. 13(f) has an intercept of 1.37982 GHz, which is basically equal to the initial resonant frequency, and then the strain factor was converted into micro-strain units with a sensitivity of 1.90909 kHz/$\mu\varepsilon$. The corresponding fitted linear can be calculated as follows:

$$\text{Fre}-\text{X} = 1.00273Ku + 1.37982 \tag{11}$$

$$\text{Fre}-\text{Y} = -1.90909Ku + 1.39636. \tag{12}$$

In this work, the strains performance of the integrated sensor is evaluated comprehensively by analyzing the resonant frequency variation trend of the rectangular microstrip patch and the 4-bit coupling encoding resonators. The simulation shows that considering the Poisson effect, when the integrated sensor is subjected to unidirectional tension or pressure, the longitudinal strain will also cause the transverse strain, and the sensitivity of the longitudinal strain is higher than that of the transverse strain. Finally, based on the transmission line model, using the basic resonant frequency of the antenna sensor with rectangular radiation patch, the fitting curve of the

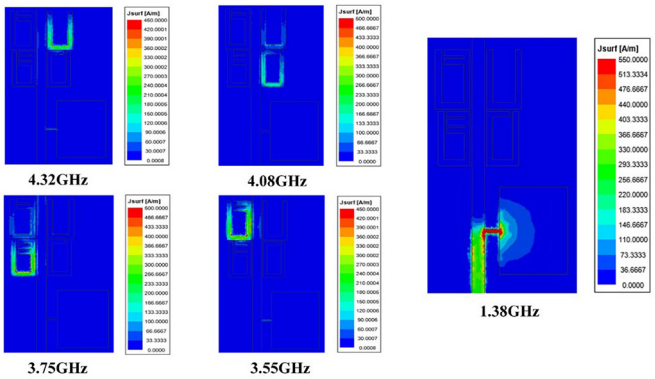

Fig. 14. Surface current distribution at different operating frequencies.

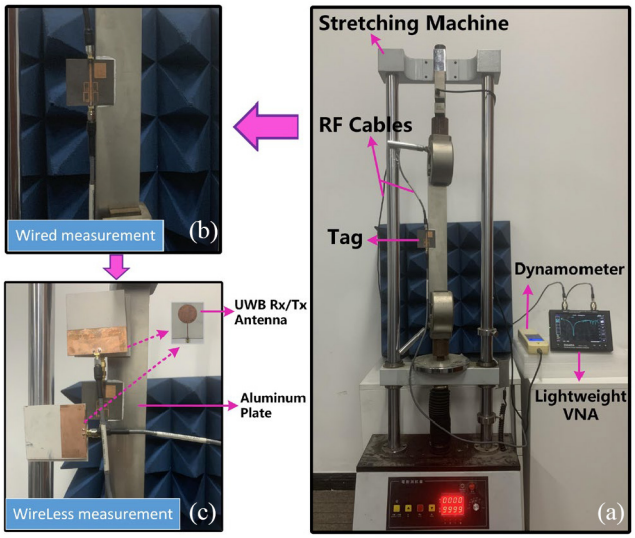

Fig. 15. Strain detection experiment scene. (a) Strain magnitude and orientation detection. (b) Wired measurement. (c) Wireless measurement based on retransmission.

relationship between the resonant frequency shift and the strain of the antenna is derived.

Fig. 14 shows the surface current distribution of the integrated sensor under different operating frequencies. It can be observed that at the operating frequency of the rectangular patch strain sensing unit, the current on the surface of the coupled U-shaped resonant coding unit is very weak. Therefore, the coupling effect of each part of the structure is small, the strain sensing function is only quantified in the defined frequency band, the strain, and coding unit functions are clearly divided without interference and the optimization parameters of the integrated sensor are reasonable.

B. Experimental Verification of Sensor Strain Behavior

Building an integrated sensor strain detection system to test the performance of the RFID strain sensor tag. The entire detection platform includes the designed RFID sensing tag, VNA, disc monopole UWB antenna, stretching machine (SJV-30000, Siwei Instrument Company, Ltd., China), and aluminum plate to be tested.

The strain experiments in this section were carried out in a tensile manner, which used the SJV-30000 tensile machine.

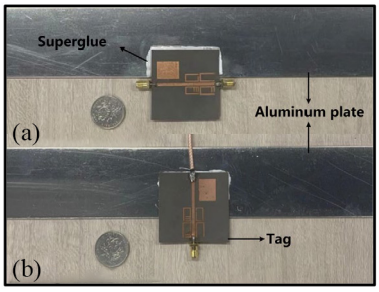

Fig. 16. Fabricated tags and superglue transfer to aluminum plate.

According to Saint Venant's Principle, in order to ensure the uniform force on both ends of the tag's strain sensing unit that adsorbed on the aluminum plate, the aluminum plate to be tested should be as long as possible, so a cuboid test specimen with a dimension of 350 mm × 50 mm × 1.5 mm was used, and its two ends were fixed on the chuck of the stretching machine, and the tensile force was applied to the aluminum plate through the change of the position of the chuck at both ends of the stretching machine. The tension value is displayed by dynamometer in real time.

The experimental scene is shown in Fig. 15, and Fig. 15(a) shows the strain magnitude and orientation detection platform based on chipless RFID tags, Fig. 15(b) and (c) shows two methods of wired measurement and wireless measurement based on retransmission are designed, respectively. As shown in Fig. 16, in the test process of the experimental scene, in order to make the sensor and the aluminum plate fit well, the surface of the aluminum plate needs to be cleaned and slightly polished. The rough surface is easier to make the superglue and the sensor closely fit on the aluminum plate. Both ends of the aluminum plate were fixed to the stretching machine, and the sensor was connected to a lightweight VNA (SYSJOINT, SV4401A) with RF cables.

In this experiment, the initial resonant frequency of the sensor was measured and uploaded at the beginning of this experiment. Then, starting from 0 kN, a tensile force with a span of approximately 2 kN is applied to the aluminum plate, and the actual tensile force value is recorded after the dynamometer reading is stable. Considering the influence of objective reasons, such as laboratory manufacturing process, test, and experimental instrument accuracy, there are inevitable errors in the experimental test process, and the initial resonance frequency of the tag's strain unit is also bit different from the simulation dimension. Therefore, this article focuses on the variation trend of strain resonance frequency.

The experimental measurement results record the strain data of the lightweight VNA and the conventional VNA under the wired measurement, respectively. Meanwhile, in order to compare the loss in the wireless detection, this work also records the strain data of the lightweight VNA under the wireless measurement based on retransmission. In an ideal case, the amount of strain generated under tension can be calculated as follows:

$$\varepsilon_t = \frac{F_t}{E_{\text{eff}} \times A} \tag{13}$$

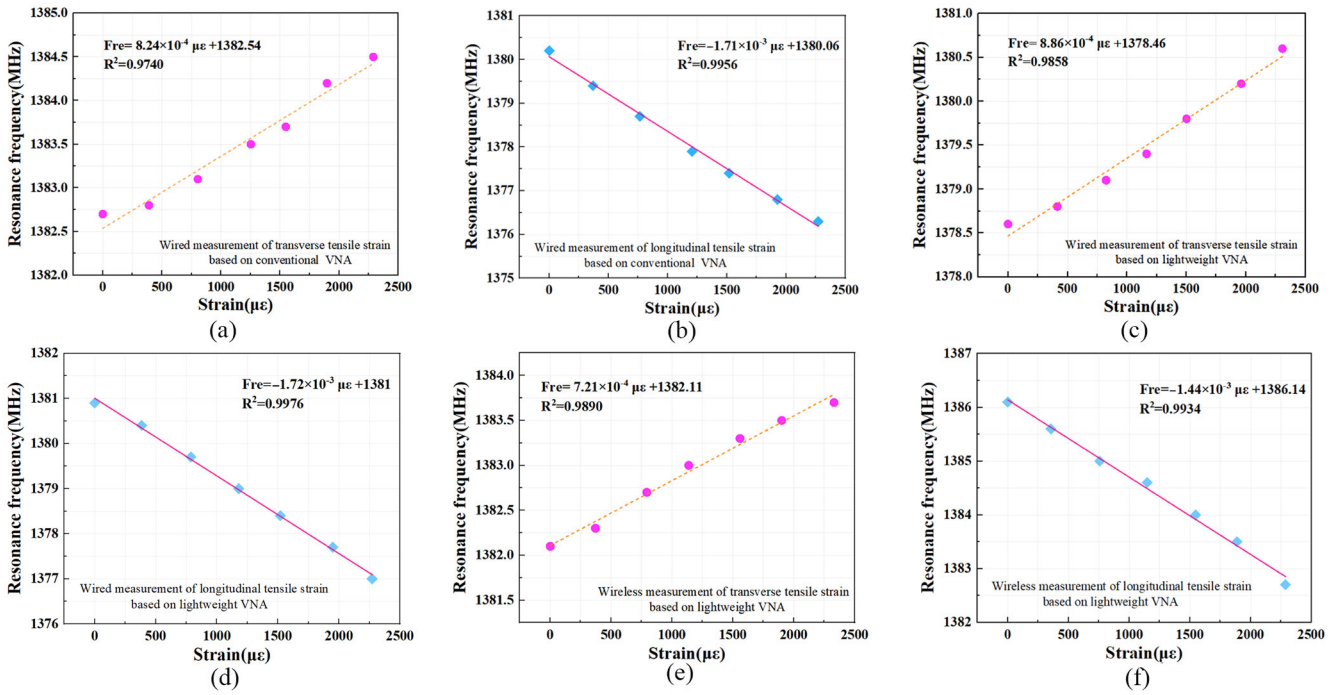

Fig. 17. Linear fitting line, (a) wired measurement of transverse tensile strain frequency shift based on conventional VNA, (b) wired measurement of longitudinal tensile strain based on conventional VNA, (c) wired measurement of transverse tensile strain frequency shift based on lightweight VNA, (d) wired measurement of longitudinal tensile strain frequency shift based on lightweight VNA, (e) wireless measurement of transverse tensile strain frequency shift based on lightweight VNA, and (f) wireless measurement of longitudinal tensile strain frequency shift based on lightweight VNA.

where F_t is the tensile force, ε_t is the tensile strain, E_{eff} is the elastic modulus of the aluminum plate ($E_{\text{eff}} = 70$ Gpa), and A is the cross-sectional area of the aluminum plate, which is 1.5 mm $\times$ 50 mm.

As the strain mechanism of the stretching machine has a certain hysteresis, it cannot accurately stay at the expected value in the stretching behavior, and the step size of the force can only be close to the standard value. Therefore, to improve the reliability of the experiment, it is necessary to test multiple groups of controlled experiments. In the experimental measurement process, six groups of tests are performed, respectively, and each measurement was repeated three times to reveal the average errors of means. Finally, the measured strain value and the corresponding shift frequency are linearly fitted in Fig. 17 to obtain the actual strain sensitivity of the tag.

It is worth noting that the experiment is limited by the measurement range of the stretching machine and the material properties of the aluminum plate, so in fact the tag is subject to a limited range of strain values. Under the force of small strain, the dimension of the tag will change slightly, resulting in a small change in the resonant frequency shift, and the strain sensitivity will be further reduced because of the high-frequency region, so the resonant frequency of the strain unit should not be too high at the beginning of the design, which also requires the VNA to have higher sampling points and higher frequency band test performance. This experimental test is not completed in an anechoic chamber. When the UWB antenna is used for wireless measurement and communication, the interference of the surrounding structure will generate corresponding microwave noise. Meanwhile, metal equipment, such as stretching machines and fixing clips will have certain effects on the wireless detection system. Therefore, when performing a small strain measurement, the data needs to be collected more precisely, and the wireless strain measurement scenario requires a more demanding test environment.

In this work, a lightweight VNA is used to replace the traditional large VNA for strain measurement. Although it is not as good performance as traditional VNA in the number of sampling scan points and resolution, the lightweight VNA has the advantages of mobility, lightweight, and high efficiency, which makes it has a very broad prospect in engineering applications. The focus of this work is to test the sensitivity of the chipless tag's strain sensing based on lightweight VNA, and to verify that the lightweight VNA can be used as a lightweight alternative to traditional VNA under the condition of certain accuracy.

C. Strain Behavior of Tags Based on Flexible Substrates

With the maturity of the flexible circuit board processing technology, the planar flexible RFID antenna produced in batches based on this substrate can be easily applied to SHM. The flexible substrate allows RFID tags to be placed on the complex surface of objects, providing more flexible placement measures. Therefore, in this part of the work, we use Rogers 3003 ($\varepsilon_r = 3$, $h = 0.75$ mm, $\tan\delta = 0.0013$) with similar performance to Rogers 5880 ($\varepsilon_r = 2.2$, $h = 0.78$ mm, $\tan\delta = 0.0009$) as the flexible dielectric substrate. As shown in Fig. 18, a flexible integrated tag with multiencoded resonant units is fabricated and studies its strain sensing characteristics, which provides a solution for applying the RFID technology to complex mechanical structure health monitoring.

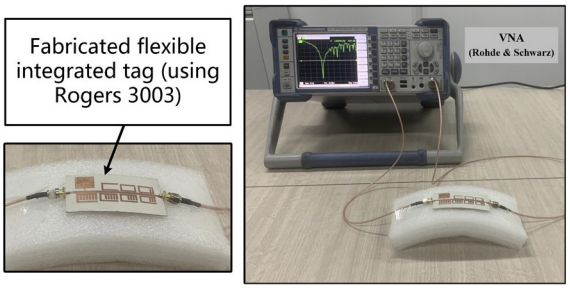

Fig. 18. Fabricated flexible integrated tags.

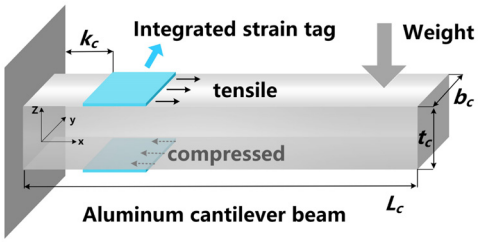

Fig. 19. Model diagram of a cantilever beam.

As shown in Fig. 19, a more simplified model was used in this study to measure the flexural strain. We set up a system consisting of a standard cantilever beam made of aluminum material to characterize the change in the resonant frequency of the tag under bending tension and compression. One end of the aluminum cantilever beam is fixed at a height of 0.75 m, and the other end carries the load. The sensor is super glued to the top of the cantilever surface, 40 mm from the fixed end. When weights are gradually added to the load end of the beam, the bending of the aluminum plate is used to apply force to the strain sensor, so that the strain experienced by the strain sensor can be calculated by (14) through elastic bending theory and Hooke's law [34]

$$\varepsilon_k = \frac{6F_c(L_c - k_c)}{E_{\text{eff}} b_c t_c^2} \tag{14}$$

where F_c is the load applied at the free end, $L_c = 450$ mm is the length of the aluminum plate, $k_c = 60$ mm is the distance from the center of the sensor to the fixed end of the aluminum plate, and $b_c = 50$ mm and $t_c = 1.5$ mm are the width and thickness of the aluminum plate, respectively. *Eeff* is the effective elastic modulus of the aluminum plate with a determined value of 70 Gpa. Therefore, for every 100-g weight applied to the heavy end of the aluminum plate, the deformation of the strain sensor increases by about 0.0297%.

The strain characterization test based on the cantilever beam setup is shown in Fig. 20. It is worth noting that the compressive strain is measured by subverting the position of the tag on the downwardly inclined cantilever beam. To verify the reliability of the measurement system and reduce random errors, multiple cycles of repeated measurements were undertaken, and their mean were used for sensitivity calculations. In the experimental test process, a lightweight Lite-VNA is used to connect the personal computer (PC) for real-time data transmission and collection and to keep the aluminum beam working within its elastic range, the load of the weight

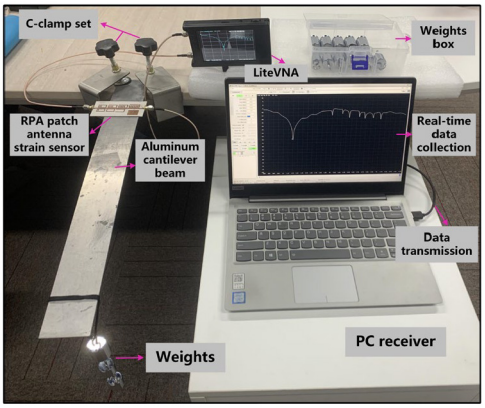

Fig. 20. Strain characterization test based on cantilever beam setup.

is limited to within 600 g. For purpose of counteracting the instability caused by the oscillation of the aluminum plate at each loading of 100 g, and each strain measurement needs to be collected after the cantilever is stationary. In addition, we used the conventional high-precision VNA for measurement and comparative analysis.

The normalized magnitude of resonant frequency shift ΔFre (ppm) in percentage can be represented in (15) as follows:

$$\Delta\text{Fre} = \frac{\left(f_o^{\text{initial}} - f_n^{\text{shift}}\right)}{f_0^{\text{initial}}} \times 10^6. \tag{15}$$

The experimentally measured tensile and compressive strain results in different directions are present in Fig. 21, and the measured results are consistent with the derived strain theory. When the longitudinal tensile strain increases, the resonance frequency of the RPA unit decreases, and with the longitudinal compression increases, the resonance frequency shifts to a higher direction. When the transverse tensile strain increases, the resonance frequency of the RPA unit increases, and with the transverse compression increases, the resonance frequency shifts to a smaller direction. In contrast, the number of scanning points of the traditional VNA is four times that of the lightweight Lite-VNA in the same frequency band measurement range, but scanning more sampling points will bring more noise, and the resonance curve needs to be further optimized.

In this work, the spectrum of fabricated flexible tags was extracted using traditional VNA and lightweight VNA, respectively. It is worth noting that the tags based on the flexible substrate can be easily bent with the bending of the aluminum plate, and within a small strain range, the tags can be recycled. During the experimental measurement, it is found that the resonance frequencies of encoding units of the tags also create different degrees of shifting, which are greater than the value under the plane strain condition. However, compared with the RPA unit, the frequency shift effect of the encoding units is smaller, and is linearly irregular. Therefore, the resonance frequencies of the encoding units can be quantized within a predetermined frequency band.

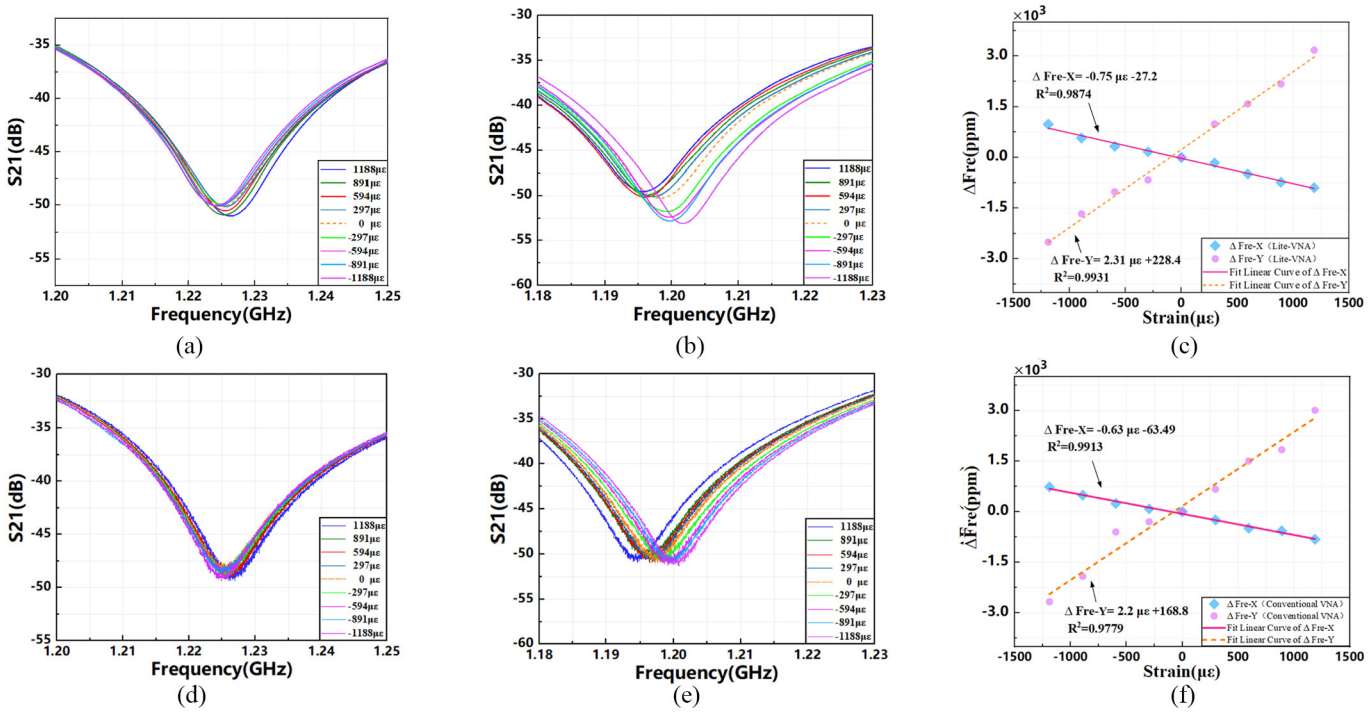

Fig. 21. (a) S21 curve shift of the strain unit after transverse strain based on Lite-VNA. (b) S21 curve shift of the strain unit after longitudinal strain based on Lite-VNA. (c) Linear fitting line of transverse strain frequency shift based on Lite-VNA. (d) S21 curve shift of the strain unit after transverse strain based on conventional VNA. (e) S21 curve shift of the strain unit after longitudinal strain based on conventional VNA. (f) Linear fitting line of longitudinal strain frequency shift based on conventional VNA.

D. Temperature Dependent Analysis

The antenna tag proposed in this article has good strain shift characteristics and flexible design for SHM application, since engineering applications require the tags to working in a climate varying environment, so testing the temperature dependence of the tag is helpful to improve the detection accuracy and robustness of the strain integrated sensor. As shown in Fig. 22, we attach the tags of two different substrates on the temperature-controlled heater, and the temperature sensitivity of its resonance frequency with temperature change was tested. In this work, temperature measurement did not exceed 120 °C, and the test results showed that the tags based on the Rogers3003 flexible dielectric substrate was little affected by temperature changes, and the frequency shift was less than 1 MHz. On the contrary, the overall resonance frequency response of the tag based on the Rogers5880 dielectric substrate increased with temperature increases.

The Influence of the tag by the external temperature on the strain characteristics is not the mainly focus of this study, therefore no further analysis was performed.

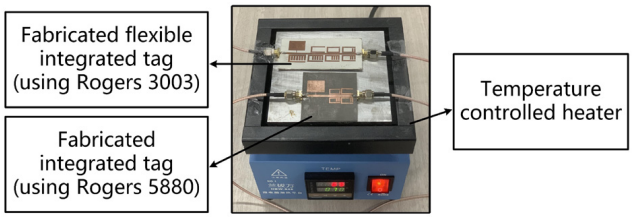

Fig. 22. Temperature dependence test of resonance frequency of tag antenna.

V. Prospect for Tunable Encoding Strain Tag

In this article, the proposed chipless RIFD integrated tags can be installed in remote areas as well as large-scale applications in economically developed areas. Passive RFID electronic tags are easy to print and further integrate, so they can be flexibly embedded in active sensing systems and deployed in areas where economic conditions permit.

The spectrum resources of sensing tags are very limited, so it is a key feature to maximize the spectrum usage of the tags while reducing the cost. In general, the encoding information carried by the chipless RFID sensor are unchangeable after fabricating. However, in the case of easy access to power, by integrating an RF switch with electronic control characteristics on the encoding resonators, the frequency reconfigurability of the encoding units of the tag can be achieved, which expand the application scenarios of the proposed tags [35].

The encoding characteristics of the electronic tag can be controlled by an embedded microcontroller unit (MCU) connected to all RF switches. MCU as the core control multichannel switch ON/OFF processing. At the same time, the MCU can be configured with multiple input/output (IO) interfaces for easy connection to other digital or analog electronic sensors. When there is a large amount of data to be processed, the ordinary MCU is often not easy to meet the requirements for multichannel analog-to-digital (A/D) control and data processing due to the influence of the

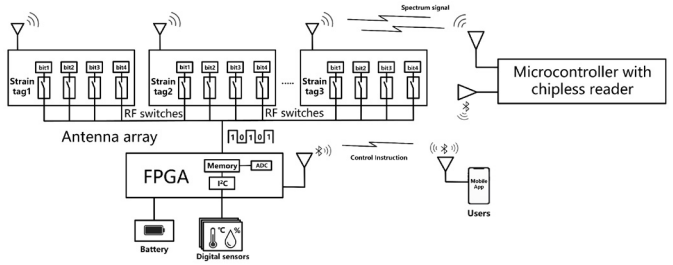

Fig. 23. Schematic of electronically tunable strain tags sensing system.

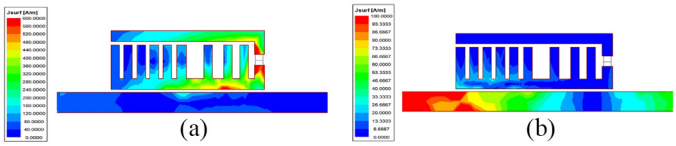

Fig. 24. Surface current distribution of a single encoding resonator. (a) ON state. (b) OFF state.

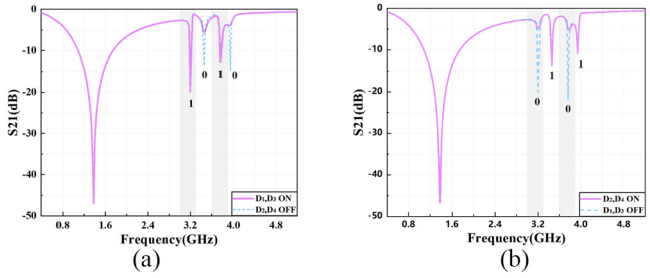

Fig. 25. Tuning state of integrated sensor encoding. (a) 1010 state. (b) 0101 state.

instruction cycle and processing speed of the MCU itself. Therefore, field programmable gate array (FPGA) can be used to replace MCU to improve the efficiency of multisignal processing [36].

In Fig. 23, we propose a schematic of the integrated design of electronically tunable strain tags for SHM coverage in economically developed regions. We use FPGA to reconfigure the encoding capacity of the tag and use the Bluetooth communication module for intelligent interaction with the users. Users can complete the configuration of the coding capacity of the tag through the mobile APP. FPGA can connect other electronic sensor through the IO interface to realize real-time monitoring of various sensing parameters. In addition, a microcontroller with a chipless reader is used to extract spectral data between the strain antenna tag array. The microcontroller sends the collected spectrum data to the users.

To simulate the controllability of the encoded tags printed on the dielectric substrate, this work sets up the lumped circuit elements of an equivalent PIN diode (SMP1340-079LF) in ANSYS software [37], which as a low loss RF switch. The RF switch is set in the middle of the bottom of the U-shaped slot. The characteristics of the coupled band-stop filter are adjusted by controlling the ON/OFF state of the RF switch. Each coupled multibranch U-shaped resonant unit is represented by an inductor L, a resistor R, and a capacitor C in parallel. In the ON state, they act as conductors, and current is carried across the interconnect, making the structure a complete coupled band-stop filter. In the OFF state, the switch acts as an insulator, cutting off the current in the resonator.

The band resistance variation of the filter can be explained by the surface current distribution, as shown in Fig. 24. Ideally, when the RF switch is turned on, the current flows in the whole U-shaped groove, and there is also some current on the branches inside the groove. The configuration of branches changes the electrical length of the U-shaped resonator, so the frequency of the resonant unit will be shift. On the contrary, when the RF switch turns off, the current cannot pass through the upper part of the U-groove. At this time, the length of the U-groove electrical radiation changes significantly, the resonant frequency will produce a large shift, and the original resonant frequency disappeared, to achieve the purpose of encoding reconfigurable. In the actual welding, due to the U-shaped resonator coupling connection, no additional bias circuit is required to isolate the dc signal, which can reduce the complexity of electronic tuning integration.

The simulation of the encoding units of the integrated sensor sets four PIN diode switches, D1, D2, D3, and D4, respectively. Due to the coupling feeding, the structure is only used for the encoding resonance unit and has no effect on the main transmission line and the subsequent strained rectangular patch. The S21 response curve in the ANSYS software is shown in Fig. 25, Fig. 25(a) shows that D1 and D3 are turned on, D2 and D4 are turned off, and the corresponding coding state is 1010. Fig. 25(b) shows that D2 and D4 are turned on, D1 and D3 are turned off, and the corresponding coding state 0101 is reached. It can be seen that the encoded resonance units have good tunability, but the resonant frequencies of the four encoding units have a certain frequency shift effect after RF switch is set. Considering that the size of the resonator is reduced after the integration, but the size of the simulated PIN diode switch is copied according to the real PIN diode model, the setting of the open slot reduces the radiated electrical length of the antenna to a certain extent, thus causing a certain shift, so it is necessary to use a smaller RF switch for simulation.

Herein, we propose a new strategy to fabricate strain tags with good flexibility and tunable encoded information. Compared with traditional NDT-based strain patches sensors, this work designs a high capacity with tunable encoded strain tag, and proposes a more simplified and more smart detection method, which has lower power consumption requirements and efficient multisensor data transmission modes.

VI. Possible Lightweight Detection Strategy

The chipless RFID tag antenna can be regarded as a sensor module when detecting structural strain, and the physical quantity of the characteristic to be measured is coupled with the geometric structure and effective radiation electrical characteristics of the tag antenna. The main challenge of the RFID metal strain integrated sensor proposed in this article is the balance between resistance to metal interference with the sensing communication performance. In addition, it is equally important to develop a portable reader for chipless RFID tag detection.

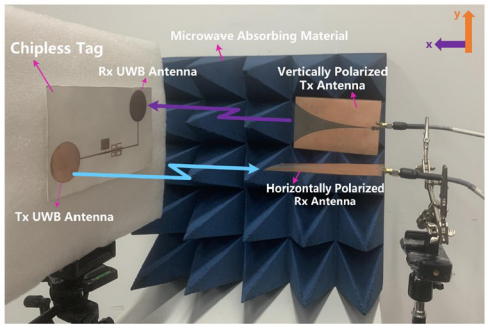

Fig. 26. Wireless measurement based on retransmission.

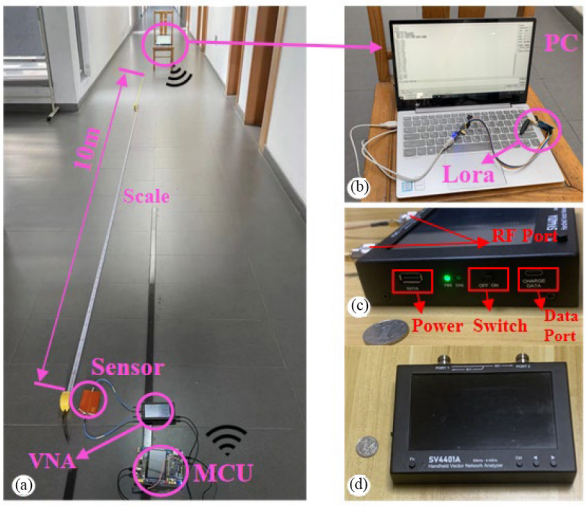

Fig. 27. Low cost testing methods. (a) Wireless transmission test for chipless RFID tag. (b) PC control side. (c) Low cost reader device interface. (d) Low cost reader front view.

In engineering structures, complex environments will produce different degrees of electromagnetic interference, which will increase the difficulty of extracting characteristic parameters of the tags. As shown in Fig. 26, the RFID tag uses the transmission coefficient (S21) based on retransmission to replace the backscatter technology, which has more stable communication performance in complex background noises. To achieve a longer wireless transmission distance, we design the high gain wideband Vivial antenna as a transceiver antenna matched to the VNA. Moreover, SHM is typically targeted at public infrastructure, such as high-rise steel frame buildings, large bridges, communication towers, and large wind power towers. Sensors need to be deployed in different locations, usually in cascades, to cover a larger structural area. Consider the above factors, it is extremely difficult for a reader placed in a fixed position to accurately communicate with so many sensors. In sensor networks, the extraction and classification strategies of sensor data are also highly required, which needs to transmit massive sensor data to the server for further processing over a long distance.

In order to realize a more economical and flexible detection method, this article proposes a novel sensing tag detection strategy that using the lightweight chipless RFID reader combined a the microcontroller, which communicates the microcontroller with the lightweight reader, the real-time extraction

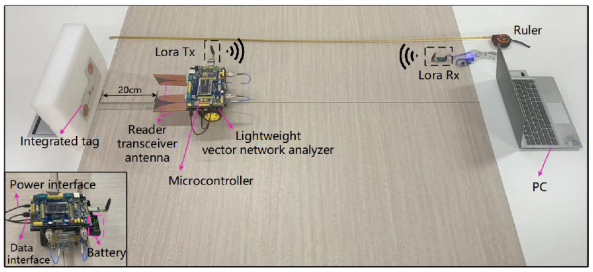

Fig. 28. Wireless measurement based on retransmission.

of the transmission parameter (S21) of the chipless RFID tag can be realized. The microcontroller can also control the working state of the lightweight reader, and use the communication module to realize the flexible network access mechanism, realize the intelligent extraction and wireless transmission of sensing data, and provide a means to solve the problem of short reading distance of chipless technology.

In Fig. 27, the whole process of chipless RFID tag parameter wired extraction and wireless transmission. First, the PC sends a work command, and the microcontroller receives the command to wake up the lightweight VNA and provide power for it. The sensor is wired to the VNA through a copper coaxial cable. The VNA extracts the S21 parameter of the tag and transmits it to the microcontroller. Then, the high-sensitivity radio transceiver LoRa module (SX1276, Semtech) that equipped with microcontroller send the data to the PC for analysis and processing. Finally, the PC restores the spectrum information of S21 parameters of the sensor. Fig. 27(b) is the display interface of real-time receiving tag S21 amplitude information on PC. Fig. 27(c) and (d) are a lightweight VNA (SV4401A and SYSJOINT), whose size is 190 mm $\times$ 130 mm $\times$ 30 mm and working frequency range from 50 kHz to 4.4 GHz and the transmission parameter dynamic range is greater than 50 dB. The LoRa module can stalely transmit data for a long distance beyond 1 km.

Although the traditional large microwave network analyzer has many advantages in measuring accuracy and integration of various functions, it has limitations, such as large size, heavy weight, and high detection cost. Thus, the intelligent detection method based on lightweight VNA is more economical and flexible method with application value in IoT and SHM.

In contrast, there are also many reports and applications about low-cost detection methods based on universal software radio peripheral (USRP) [38], but the lightweight detection method proposed in this article possibly has more potential. In Fig. 28, we connect the microcontroller to the lightweight VNA and install it on a movable pallet trolley to collect characteristic parameters from the fixed sensor. The lithium battery in the pallet trolley supplies power to the entire detection device.

In this work, the microcontroller and lightweight VNA can be further embedded and integrated, work without a high power supply, and freely switch between working and sleeping states, while the USRP consumes a high power due to the large number of algorithms and programs that need to be processed. Therefore, the chipless RIFD detection method proposed in this article focuses on data acquisition and transmission, which cannot process and analyze massive data in real time.

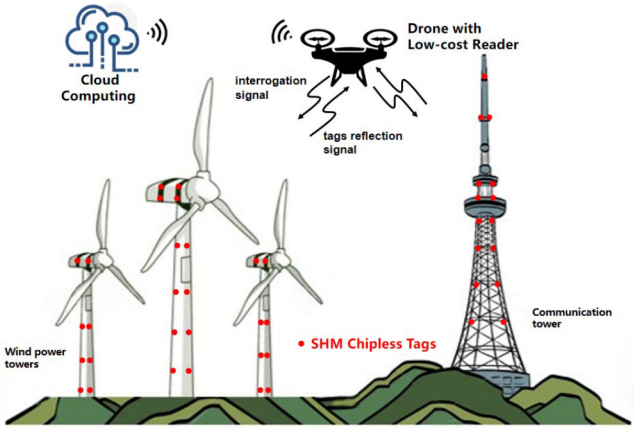

Fig. 29. Possible low-cost wireless strain sensing systems for SHM.

In the future, Drones can carry this low power consumption and networkable detection device, flying to any location the user wants to interrogate the SHM sensors in real time as shown in Fig. 29. Users extract their health status information by scanning the deployed sensors network, and simultaneously analyze the encoded information carried on the sensors to assist the unmanned aerial vehicle (UAV) in positioning and tracking. All collected data can be sent to the cloud server for data processing and sharing, and administrators can also access the cloud server for further flexible processing to achieve the purpose of dynamic monitoring.

VII. Conclusion

In this article, a novel chipless RFID system with high capacity encoding and strain sensing is presented in SHM application. To realize large-scale commercial deployment on key position of metal structures, a novel RFID strain integrated tag and its low-cost intelligent detection method are designed. The integrated tag can set more compact resonant encoding in the working frequency band. A U-shaped resonator with a high Q value and multistate coupling line is designed, which effectively increases the encoding capacity by flexibly adjusting its internal metal branches. Meanwhile, rectangular patches with well-normalized frequency shift characteristics are used for strain measurement of metal installed. Furthermore, the proposed passive tag possesses flexible-strain properties and is easy to print and embed, so it can be further integrated in active sensing systems to realize RFID wireless strain sensing, which is crucial for the IoT and this integrated tag is a good product for large-scale deployment in SHM. Finally, based on the tag design, a low-cost RFID mobile detection scenario is proposed, the feature parameters of tags are extracted by wireless measurement based on retransmission and wireless data transmission for long distance, which verifies the great prospect of this smart RFID system in SHM engineering application, and provides a new cost-effective IoT nondestructive detection strategy.

References

[1] C. A. Tokognon, B. Gao, G. Y. Tian, and Y. Yan, "Structural health monitoring framework based on Internet of Things: A survey," *IEEE Internet Things J.*, vol. 4, no. 3, pp. 619–635, Jun. 2017.

[2] A. Moallemi, A. Burrello, D. Brunelli, and L. Benini, "Exploring scalable, distributed real-time anomaly detection for bridge health monitoring," *IEEE Internet Things J.*, vol. 9, no. 18, pp. 17660–17674, Sep. 2022.

[3] F. Hernandez-Valle, A. R. Clough, and R. S. Edwards, "Stress corrosion cracking detection using non-contact ultrasonic techniques," *Corrosion Sci.*, vol. 78, pp. 335–342, Jan. 2014.

[4] J. Gubbi, R. Buyya, S. Marusic, and M. Palaniswami, "Internet of Things (IoT): A vision, architectural elements, and future directions," *Future Gener. Comput. Syst.*, vol. 29, no. 7, pp. 1645–1660, 2013.

[5] G. Y. Tian, Y. He, I. Adewale, and A. Simm, "Research on spectral response of pulsed eddy current and nde applications," *Sens. Actuators Phys.*, vol. 189, pp. 313–320, Jan. 2013.

[6] G. C. Wan, M. M. Li, Y. L. Yang, L. Xie, and L. Chen, "Patch-antenna-based structural strain measurement using optimized energy detection algorithm applied on USRP," *IEEE Internet Things J.*, vol. 8, no. 9, pp. 7476–7484, May 2021.

[7] A. Sharif et al., "Low-cost inkjet-printed UHF RFID tag-based system for Internet of Things applications using characteristic modes," *IEEE Internet Things J.*, vol. 6, no. 2, pp. 3962–3975, Apr. 2019.

[8] A. Burrello, A. Marchioni, D. Brunelli, S. Benatti, M. Mangia, and L. Benini, "Embedded streaming principal components analysis for network load reduction in structural health monitoring," *IEEE Internet Things J.*, vol. 8, no. 6, pp. 4433–4447, Mar. 2021.

[9] A. Akbari, S. Mirshahi, and M. Hashemipour, "Comparison of RFID system and barcode reader for manufacturing processes," in *Proc. IEEE 28th Can. Conf. Elect. Comput. Eng. (CCECE)*, 2015, pp. 502–506.

[10] N. Huang, J. Chen, and Z. Ma, "High-Q slot resonator used in chipless tag design," *Electronics*, vol. 10, no. 9, p. 1119, 2021.

[11] N. Javed, M. A. Azam, I. Qazi, Y. Amin, and H. Tenhunen, "A novel multi-parameter chipless RFID sensor for green networks," *AEU Int. J. Electron. Commun.*, vol. 128, Jan. 2021, Art. no. 153512.

[12] X. Yi, C. Cho, J. Cooper, Y. Wang, M. M. Tentzeris, and R. T. Leon, "Passive wireless antenna sensor for strain and crack sensing—Electromagnetic modeling, simulation, and testing," *Smart Mater. Struct.*, vol. 22, no. 8, 2013, Art. no. 085009.

[13] C. Cho, X. Yi, D. Li, Y. Wang, and M. M. Tentzeris, "Passive wireless frequency doubling antenna sensor for strain and crack sensing," *IEEE Sensors J.*, vol. 16, no. 14, pp. 5725–5733, Jul. 2016.

[14] M. Herbko, P. Lopato, G. Psuj, and P. Rajagopal, "Application of selected fractal geometry resonators in microstrip strain sensors," *IEEE Sensors J.*, vol. 22, no. 13, pp. 12656–12663, Jul. 2022.

[15] D. Li and Y. Wang, "Thermally stable wireless patch antenna sensor for strain and crack sensing," *Sensors*, vol. 20, no. 14, p. 3835, 2020.

[16] S. Dey, R. Bhattacharyya, S. E. Sarma, and N. C. Karmakar, "A novel "smart skin" sensor for chipless RFID-based structural health monitoring applications," *IEEE Internet Things J.*, vol. 8, no. 5, pp. 3955–3971, Mar. 2021, doi: 10.1109/JIOT.2020.3026729.

[17] S. Deif and M. Daneshmand, "Multiresonant chipless RFID array system for coating defect detection and corrosion prediction," *IEEE Trans. Ind. Electron.*, vol. 67, no. 10, pp. 8868–8877, Oct. 2020.

[18] C. Herrojo, J. Mata-Contreras, F. Paredes, A. Núñez, E. Ramon, and F. Martín, "Near-field chipless-RFID system with erasable/programmable 40-bit tags inkjet printed on paper substrates," *IEEE Microw. Wireless Compon. Lett.*, vol. 28, no. 3, pp. 272–274, Mar. 2018.

[19] T. Athauda and N. C. Karmakar, "The realization of chipless RFID resonator for multiple physical parameter sensing," *IEEE Internet Things J.*, vol. 6, no. 3, pp. 5387–5396, Jun. 2019.

[20] W. M. Abdulkawi and A. F. A. Sheta, "K-state resonators for high-coding-capacity chipless RFID applications," *IEEE Access*, vol. 7, pp. 185868–185878, 2019.

[21] W. M. Abdulkawi and A. F. A. Sheta, "Chipless RFID sensors based on multistate coupled line resonators," *Sensors Actuators A Phys.*, vol. 309, Jul. 2020, Art. no. 112025.

[22] A. M. J. Marindra and G. Y. Tian, "Chipless RFID sensor tag for metal crack detection and characterization," *IEEE Trans. Microw. Theory Techn.*, vol. 66, no. 5, pp. 2452–2462, May 2018.

[23] W. He et al., "Integrated textile sensor patch for real-time and multiplex sweat analysis," *Sci. Adv.*, vol. 5, no. 11, 2019, Art. no. eaax0649.

[24] S. Kang, V. P. Rachim, J.-H. Baek, S. Y. Lee, and S.-M. Park, "A flexible patch-type strain sensor based on polyaniline for continuous monitoring of pulse waves," *IEEE Access*, vol. 8, pp. 152105–152115, 2020.

[25] K. Pan, L. Teng, L. Ting, X. Zhou, A. A. Stokes, and Z. Hu, "Soft wireless battery-free UHF RFID stretchable sensor based on microfluidic technology," *IEEE J. Radio Freq. Identification*, vol. 3, no. 4, pp. 252–258, Dec. 2019.

[26] H. Cao et al., "Development and characterization of a novel interdigitated capacitive strain sensor for structural health monitoring," *IEEE Sensors J.*, vol. 15, no. 11, pp. 6542–6548, Nov. 2015.
[27] A. Vena, L. Sydänheimo, M. M. Tentzeris, and L. Ukkonen, "A fully inkjet-printed wireless and chipless sensor for CO_2 and temperature detection," *IEEE Sensors J.*, vol. 15, no. 1, pp. 89–99, Jan. 2015.
[28] V. Mulloni and M. Donelli, "Chipless RFID sensors for the Internet of Things: Challenges and opportunities," *Sensors*, vol. 20, no. 7, p. 2135, 2020.
[29] S. Preradovic and N. C. Karmakar, "Multiresonator based chipless RFID tag and dedicated RFID reader," in *Proc. IEEE MTT-S Int. Microw. Symp.*, 2010, pp. 1520–1523.
[30] G. Chakaravarthi et al., "Reusable passive wireless RFID sensor for strain measurement on metals," *IEEE Sensors J.*, vol. 18, no. 12, pp. 5143–5150, Jun. 2018.
[31] A. Lázaro et al., "Chipless dielectric constant sensor for structural health testing," *IEEE Sensors J.*, vol. 18, no. 13, pp. 5576–5585, Jul. 2018.
[32] G. Wan, M. Li, M. Zhang, L. Kang, and L. Xie, "A novel information fusion method of RFID strain sensor based on microstrip notch circuit," *IEEE Trans. Instrum. Meas.*, vol. 71, pp. 1–10, 2022.
[33] G. C. Wan, K. Xue, R. X. Gao, J. Y. Lv, and M. S. Tong, "A rectangular microstrip patch antenna used for structural health monitoring," in *Proc. IEEE Int. Symp. Antennas Propag. USNC/URSI Nat. Radio Sci. Meeting*, 2018, pp. 695–696.
[34] L. Wang, K. L. Chung, W. Zong, and B. Feng, "A highly sensitive microwave patch sensor for multidirectional strain sensing based on near orthogonal modes," *IEEE Access*, vol. 9, pp. 24669–24681, 2021.
[35] V. Arun et al., "N-shaped frequency reconfigurable antenna with auto switching unit," *Appl. Comput. Electromagn. Soc. J.*, vol. 33, no. 6, pp. 710–713, 2018.
[36] J. Chen et al., "Direction finding of linear frequency modulation signal in time modulated array with pulse compression," *IEEE Trans. Antennas Propag.*, vol. 68, no. 1, pp. 509–520, Jan. 2020.
[37] N. Pournoori, "Wireless monitoring of a charge storage in an RF energy harvesting device," M.S. thesis, Dept. Comput. Sci., Tampere Univ. Technol., Tampere, Finland, 2018.
[38] K. Tang et al., "A highly integrated passive wireless sensing system with synchronized data streaming of multiple tags," *IEEE Internet Things J.*, vol. 9, no. 17, pp. 15525–15537, Sep. 2022.

Lan Chen received the M.S. degree in signal and information processing from Tongji University, Shanghai, China, in 2004, and the Ph.D. degree in astronomical technology and method science from Shanghai Astronomy, Chinese Academy of Sciences, Shanghai, in 2010.

She is currently a Professor with the Shanghai Institute of Technology, Shanghai, and serves as the Associate Dean of the School of Electrical and Electronic Engineering. Her current research interests include high-speed digital signal processing, digital terminal technology research, and signal simulation technology.

Luyi Liu received the B.S. degree in electrical engineering and its automation from Shanghai University of Electric Power, Shanghai, China, in 2020. He is currently pursuing the M.Sc. degree in control science and engineering with the Shanghai Institute of Technology University, Shanghai.

His current research interests include multiparameter sensor design based on RFID detection systems, reconfigurable antenna design, and wireless sensor network.

Lei Kang received the B.S. degree in electrical engineering and its automation from Hebei University, Baoding, China, in 2019. She is currently pursuing the M.Sc. degree in control science and engineering with Shanghai Institute of Technology University, Shanghai, China.

Her current research interests include multiparameter sensor design-based RFID detection systems and structural health monitoring.

Zhichong Wan received the B.S. degree in electronic information engineering from Nanchang University, Nanchang, Jiangxi, China, in 2019. He is currently pursuing the M.Sc. degree in control science and engineering with Shanghai Institute of Technology, Shanghai, China.

His current research interests include machine learning and embedded development.

Guochun Wan received the Ph.D. degree in transportation information engineering and control from Tongji University, Shanghai, China, in 2011.

He became an Associate Professor with the Department of Electronic Science and Technology, Tongji University. His current research interests include signal and information processing, with an emphasis on error-correcting coding, RFID sensor, and system-on-chip design for communications and coding theory applications.

Liyu Xie received the B.S. and M.S. degrees in mechanical engineering from Tongji University, Shanghai, China, in 2000 and 2003, respectively, and the Ph.D. degree in system design engineering from Keio University, Tokyo, Japan, in 2009.

In 2019, he became an Associate Professor with the College of Civil Engineering, Tongji University. His current research focuses on smart sensors, structural health monitoring, and structural vibration control.